PERGAMON

International Journal of Heat and Mass Transfer 44 (2001) 4047–4058

International Journal of HEAT and MASS TRANSFER

www.elsevier.com/locate/ijhmt

Simulation of fully developed laminar heat and mass transfer in fuel cell ducts with different cross-sections

Jinliang Yuan, Masoud Rokni, Bengt Sundén *

Division of Heat Transfer, Lund Institute of Technology, P.O. Box 118, S-22100 Lund, Sweden

Received 1 February 2000; received in revised form 2 January 2001

Abstract

The fully developed laminar flow and heat transfer for ducts with rectangular and trapezoidal cross-section in fuel cells have been numerically simulated with one porous wall with a uniform mass injection or suction, the other three walls being impermeable. The new concept of thermal boundary conditions of combined constant heat flux and constant temperature on the walls was implemented. Based on the constant thermal–physical property assumption, the wall friction factor and Nusselt number for different mass transfer rates, the aspect ratios and base angles are obtained. Comparisons of these numerical results with published data are also presented.

1. Introduction

Fuel cells continuously convert chemical energy to electrical energy through electrochemical reactions at the anode and cathode. There are sources of heat generation and absorption in fuel cells, which have effects on the distribution of temperature and gas flow rate. At an operating temperature of about 1000°C and pressures greater than one atmosphere, solid oxide fuel cells (SOFCs) are the obvious choice [1]. Different coefficients of thermal expansion, interdiffusion of the materials used for the anode, electrode and cathode, and stresses caused by temperature gradients are the major engineering problems faced in the design of SOFCs [2]. The modeling of heat and mass transfer in SOFCs is becoming crucial and important for the successful design and operation of the SOFC system.

Several fundamental studies of flow characteristics in ducts with different cross-sections exist in the literature. Most of the recent studies concern turbulent flow in ducts, e.g., Rokni and Sundén [3] and Rokni [4] simulated turbulent gas flow and heat transfer in ducts with different cross-sections using different turbulence models. The thermal boundary condition of either constant temperature or constant heat flux on all walls was implemented in these studies, not a combination which is the case in this investigation.

Analytical or empirical expressions for the heat transfer coefficients and friction factor are available in the literature for simple geometries and the wall boundary conditions of constant wall heat flux or constant wall temperature, see [5–7]. However, as will be clarified in this paper, the wall boundary conditions for fuel cell ducts are quite unique and need careful consideration.

During recent years, a number of investigations concerning mathematical modeling have been presented for simulation of the heat transfer and gas flow in SOFCs [8–13]. Vayenas et al. [8] created a two-dimensional mixing cell model for cross-flow to simulate the distribution of gas species, temperature, and current density. For the gas streams, the convective heat transfer coefficient $h_f\ (=h_a)=0.253/D_h$ was employed. Ahmed et al. [9] assumed fully developed laminar flow with a Nusselt number value of 3.0 for convective heat transfer between the gases and the solid surfaces. The generated heat was considered to be created in the electrolyte layer. The boundary conditions considered in the work of Ferguson et al. [10] are based on the idea that the cell is part of a whole stack and that the overall behavior is

* Corresponding author.
E-mail address: bengt.sunden@vok.lth.se (B. Sundén).

0017-9310/01/$ - see front matter
PII: S0017-9310(01)00052-7

Nomenclature

A	cross-section area
A_1	wetted perimeter
a	width of lower wall
b	width of upper wall
c	constant
C_p	specific heat at const. pressure
D_h	hydraulic diameter
f	Fanning friction factor
h	height of the duct
h_f	heat transfer coefficient
m	mass flow rate
Nu	Nusselt number
P	pressure
q	heat flux
Re_i	inlet Reynolds number
Re_m	wall Reynolds number
S_ϕ	source term in the general equation
T	temperature
U, V, W	velocity components in x, y and z directions, respectively
x, y, z	Cartesian coordinates

Greek symbols

α	base angle of the duct
Γ	diffusivity
λ	thermal conductivity
μ	dynamic viscosity
ν	kinematic viscosity
ρ	density
ϕ	variable

Subscripts

bulk	bulk fluid condition
f	fuel cell
i, j, k	coordinate indices
m	wall mass transfer condition
q	with constant heat flux
T	with constant temperature
w	wall condition

periodic. Periodic boundary conditions were imposed for the temperature on the top wall and bottom wall of the cell ($q_T = q_B$), while insulation conditions were imposed on the lateral walls ($q_L = 0$). In the work by Melhus et al. [11], the reduction of the mass of O_2 in the cathode chamber, consumed in the reaction with fuel, was assumed to be regained in the anode as H_2O. Adiabatic surfaces were chosen as boundary condition. Both gas flows were in developing laminar flow.

Both gaseous reactant flows at the cathode and anode are subject to fluid injection and suction along the porous interface to the electrolyte. Thus they may be simulated as flow in one-porous-wall ducts and at constant heat flux boundary condition [14]. Since both the heat transfer and the pressure drop (friction factor) are significantly affected, the fluid flow and heat transfer in channels with mass transfer in porous walls have received a great deal of attention in the past decades [14–16]. The frictional and heat transfer characteristics of fully developed laminar flow in porous tubes with constant wall temperature was simulated by Kinney [15] for the range of wall Reynolds number $-5.0 < Re_m < 20.0$. The effect of mass injection, to increase the wall friction and to decrease the wall heat transfer, was verified. Hwang et al. [14] simulated a square duct with boundary conditions of one porous wall subject to a constant heat flux, while the other three walls were adiabatic and impermeable in the range of $-20.0 < Re_m < 20.0$. Flow reversal was also observed for suction mass transfer at a critical wall Reynolds number.

As discussed above, most of the investigations deal mainly with the boundary condition of either constant temperature or constant heat flux. However, Yuan et al. [17] simulated the fully developed laminar flow in rectangular ducts with new combined thermal boundary conditions of constant heat flux at one wall and constant temperature at the other three walls. It was revealed that the Nu-number is sensitive to the wall boundary conditions.

To extend the previous work of the authors, the new approach in this paper considers the fully developed laminar flow in ducts of rectangular and trapezoidal cross-sections with one porous wall with mass transfer. The contribution of the present work is to provide mass transfer effects on the fully developed laminar flow and heat transfer under the thermal boundary condition of combined constant temperature and constant heat flux. In addition, the combined thermal boundary condition implemented in this study for ducts of different cross-sections (rectangular and trapezoidal) is unique.

2. Analysis

2.1. Problem statement

Among different types of cell stacks, there are some common main components in fuel cells, namely anode, electrolyte and cathode, which are shown in Fig. 1(a). The arbitrary duct under consideration is chosen from the fuel or the air channels and is shown schematically in Fig. 1(b). U, V and W are the velocity components in the x, y, z directions, respectively. The aspect ratio of the duct is defined as b/h. By changing this ratio and

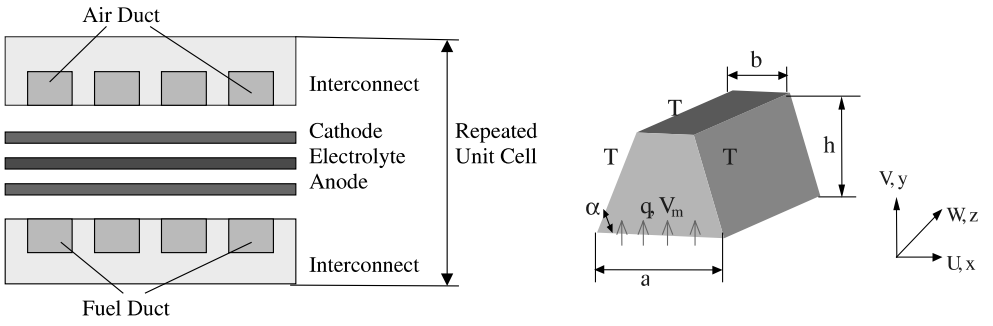

Fig. 1. (a) The structure of a unit cell, (b) schematic drawing of a duct in fuel cells.

the base angle α, different cross-sectional geometries, i.e., square, rectangular, trapezoidal ducts can be simulated.

A steady laminar flow of an incompressible fluid with constant thermophysical properties is considered. For simplicity, the following assumptions are applied.

1. The axial-velocity and -temperature distributions of the fluid at the inlet are assumed uniform.
2. The inlet Reynolds number is assumed to be Re_i $(= WD_h/v) \gg 1$, and all axial diffusion terms in the momentum equations are assumed negligible.
3. A uniform chemical reaction rate is assumed to appear in the electrolyte, which results in a uniform injection/suction to/from one wall. The released heat is taken into account by specifying a constant wall heat flux q_w at this wall.
4. The injection/suction mass transfer is assumed to be small compared to the streamwise flow.

The dimensionless injection or suction velocity on the lower porous wall can be written as [14]

$$Re_m = \frac{V_m D_h}{v}, \tag{1}$$

where Re_m is wall Reynolds number, V_m the mass transfer velocity, D_h the hydraulic diameter and v is the kinematic viscosity. In this study, Re_m is positive for injection, and negative for suction. The injection or suction fluid has the same temperature as the heated porous wall. Moreover, in SOFCs, Re_m is very small and its mean value is in the order of 1.0 for H_2O generation into the fuel channels, and O_2 consumption in the air channels. Based on this fact, the range of $-2.5 < Re_m < 2.5$ is chosen in this study which is very small compared to the main flow Re_i.

2.2. Governing equations

The governing equations of fluid flow represent mathematical statements of the conservation laws of physics. For an incompressible Newtonian fluid, these can be written as the following continuity, momentum and energy equations [5]:

$$\frac{\partial(\rho U_i)}{\partial x_i} = 0, \tag{2}$$

$$\frac{\partial(\rho U_j U_i)}{\partial x_j} = -\frac{\partial P}{\partial x_i} + \frac{\partial}{\partial x_j}\left(\mu\left(\frac{\partial U_i}{\partial x_j} + \frac{\partial U_j}{\partial x_i}\right)\right), \tag{3}$$

$$\frac{\partial(\rho U_j T)}{\partial x_j} = \frac{\partial}{\partial x_j}\left(\frac{\mu}{Pr}\frac{\partial T}{\partial x_j}\right). \tag{4}$$

2.3. Boundary conditions

The boundary conditions are

$$U = V - V_m = W = 0,$$
$$q = q_w \text{ at lower porous wall, } y = 0, \tag{5}$$

$$U = V = W = 0,\ T = T_w \text{ at other three walls.} \tag{6}$$

For the fully developed laminar flow without mass transfer, the transverse momentum equations no longer enter into the determination of the flow and temperature fields. The governing equations of momentum and temperature can then be written in the following form:

$$\nabla^2 W = \frac{\partial^2 W}{\partial x^2} + \frac{\partial^2 W}{\partial y^2} = \frac{1}{\mu}\frac{dP}{dz} = C_1, \tag{7}$$

$$q = \lambda\left(\frac{\partial^2 T}{\partial x^2} + \frac{\partial^2 T}{\partial y^2}\right) = \rho C_p W \frac{dT_{bulk}}{dz}, \tag{8}$$

where W is the axial velocity component, dP/dz and dT/dz are the pressure and temperature gradients in the main flow direction, respectively.

2.4. Additional equations

The most interesting parameters from an engineering standpoint are the friction factor and Nusselt number in the fuel cell ducts. The former one is related to the flow rate and the latter one is related to the heat exchange of the duct.

The Fanning friction factor f is defined as (see e.g., [5]):

$$f = \frac{1}{2}\frac{D_h}{\rho W_{bulk}^2}\frac{dP}{dz}, \tag{9}$$

where W_{bulk} is mean velocity of the main flow and D_h is the hydraulic diameter defined in the conventional manner. One has

$$W_{bulk} = \frac{\int W\,dA}{\int dA}. \tag{10}$$

The hydraulic diameter is defined as

$$D_h = \frac{4A}{A_1}. \tag{11}$$

dP/dz is the pressure gradient along the main stream, A is the cross-sectional area and A_1 is the wetted perimeter. When mass transfer is considered, an additional constraint to determine dP/dz in Eq. (7) can be derived from an overall mass balance. The total mass can be expressed as

$$\dot{m}_{in} + \dot{m}_m = \dot{m}_{out}, \tag{12}$$

where $\dot{m}_m$ is the mass flow rate from the porous wall. Since Re_m is assumed to be very small compared to the main flow, the above equation can then be expressed as

$$\frac{\partial W_{bulk}}{\partial z} = Re_m\frac{v}{D_h}\frac{a}{A}, \tag{13}$$

where $\partial W_{bulk}/\partial z$ is the velocity gradient in the main flow direction induced by mass transfer.

The total Nusselt number can be derived from an energy balance in the duct. Assuming that the mass flow at the porous wall is much smaller than the main stream flow, the total heat flow rate can be defined as

$$q = \rho W_{bulk} C_p A\frac{dT}{dz} - \rho C_p V_m a(T_{bulk} - T_w). \tag{14}$$

This equation can be rearranged as

$$\frac{q}{T_{bulk} - T_w}\frac{D_h}{2(a+b)\lambda} = \frac{\rho W_{bulk} C_p A(dT/dz)D_h}{2(T_{bulk} - T_w)(a+b)\lambda} - \rho C_p V_m a\frac{D_h}{2\lambda(a+b)}. \tag{15}$$

The left-hand side is the definition for the Nu and the first part on the right-hand side is the definition of the Nusselt number without mass transfer (Nu_f).

$$Nu = \frac{qD_h}{2\lambda(a+b)(T_{bulk} - T_w)}, \qquad Nu_f = \frac{\rho W_{bulk} C_p A(dT/dz)D_h}{2\lambda(a+b)(T_{bulk} - T_w)}, \tag{16}$$

where T_w, the wall temperature, is equal on three walls but varies on the fourth wall; T_{bulk} is the main flow mean temperature in the cross-section.

$$T_{bulk} = \frac{\int T|W|\,dA}{\int |W|\,dA}. \tag{17}$$

The second part of Eq. (15) is the contribution to the total Nusselt number by mass transfer. This term can be rewritten as

$$Nu_m = -PrRe_m\frac{a}{A_1}. \tag{18}$$

The total Nu is then found as

$$Nu = Nu_f + Nu_m. \tag{19}$$

3. Solution methodology

The governing differential equations are discretized into algebraic equations by a truncated Taylor series method using a finite volume method (see, e.g., [18]), and then they are solved by some iterative method.

In this study, Eqs. (7) and (8), together with the boundary conditions Eqs. (5) and (6) are solved by using a two-dimensional code, SIMPLE_HT [19]. The finite-volume method (or control-volume method), which is based on the conservation of a specific physical quantity, is used in the code. The code is designed for steady convection–diffusion problems, e.g., Navier–Stokes equations and the temperature field equation. The pressure–velocity coupling is treated by the SIMPLEC [20] method with the incompressible form of the pressure-correction equation. The convection–diffusion terms are treated by the Hybrid scheme [21]. Each variable is solved with the TDMA algorithm [21] combined with a block-correction method.

As implemented in the code, each of the differential equations can be cast into the general elliptic equation form (see, e.g., [18]):

$$\left\{\frac{\partial}{\partial x}(\rho u\phi) + \frac{\partial}{\partial y}(\rho v\phi)\right\} = \frac{\partial}{\partial x}\left(\Gamma\frac{\partial\phi}{\partial x}\right) + \frac{\partial}{\partial y}\left(\Gamma\frac{\partial\phi}{\partial y}\right) + S, \tag{20}$$

where ϕ denotes any of the dependent variables, Γ is the diffusivity and S is a source term. Once in this form, the equations are integrated over the control volumes defined on a staggered grid. The boundary conditions are introduced as source terms in control volumes neighboring boundaries whenever appropriate. The resulting system of algebraic equations is solved using an iterative method.

4. Code validation and test calculations

In order to evaluate the performance of the numerical method and code, the following test calculations have been carried out and are presented below.

4.1. Test of grid sensitivity

To check the independence of the results on the number of grid points, numerical experiments were carried out without/with injection/suction conditions and for various aspect ratios.

4.1.1. Rectangular duct

To choose a suitable mesh arrangement in a rectangular duct, some calculations with different numbers of grid points were carried out. The results for the aspect ratio $b/h = 2{:}1$ are shown in Table 1. In the table, Nu_T denotes constant temperature condition at all boundaries, Nu_q denotes constant heat flux at all boundaries, and Nu_f denotes combined constant heat flux at the porous wall (lower wall) and constant temperature at the other three walls. The table shows that the calculated Nusselt numbers do not change significantly when the number of grid points are increased beyond 60×30.

Table 1
Influence of grid size on *Nu* and *fRe* for a rectangular duct ($b/h = 2:1$) without mass transfer

Grid	*fRe*	Nu_T	Nu_q	Nu_f
20×10	14.985	3.425	4.226	3.685
30×15	15.320	3.406	4.165	3.655
40×20	15.425	3.399	4.146	3.645
50×25	15.469	3.397	4.137	3.640
60×30	15.493	3.395	4.133	3.638
70×35	15.507	3.395	4.130	3.637
80×40	15.515	3.394	4.129	3.636
90×45	15.521	3.394	4.128	3.636
100×50	15.525	3.393	4.127	3.636

Test calculations have also been carried out when mass transfer prevails at the bottom wall, for various Re_m. For example, the calculation results for mass injection or suction with $Re_m = 2.5$ with different aspect ratios are shown in Table 2. For the cases considered in this table, changes in friction factor (*fRe*) and Nusselt number (Nu_f) are less than 0.5%, if the number of grid points is further increased. By considering calculation time and accuracy, the selected number of grid points for various aspect ratios of rectangular ducts is marked by the symbol * in Table 2.

4.1.2. Trapezoidal duct

Test calculations have also been carried out for trapezoidal ducts with different aspect ratios and different base angles. As an example, Table 3 shows the results for the aspect ratio 1:1 with the base angle 60°. The table shows that 180×60 grid points may be sufficient to achieve a reasonable accuracy (based on computational time and cost) in terms of friction factor and Nusselt number. The same number of grid points is also chosen for other aspect ratios for the trapezoidal ducts.

4.2. Code performance and validation

In order to validate the performance of the computer code, it has been applied to a duct with various aspect ratios and thermal boundary conditions without mass transfer. The simulation results of these test calculations are compared with results presented in the literature, see Figs. 2 and 3.

Fig. 2 shows the calculated friction, *fRe*, for rectangular and trapezoidal ducts with different aspect ratios. The comparison shows that the computed results agree excellently with the results from the literature [7], with a maximum inaccuracy of about 2.5%. The figure shows also that at small base-angles, the friction factor remains constant when the aspect ratios are small.

Fig. 3 shows the calculated *Nu* numbers for rectangular and trapezoidal ducts with various thermal

Table 2
Test calculation for the grid sensitivity on *Nu* and *fRe* for a rectangular duct with mass transfer

Ratio (b/h)	Number of grid points	Re_m (suction)	*fRe*	Nu_f	Re_m (injection)	*fRe*	Nu_f
1:1	$30 \times 30^*$	−2.5	13.556	3.566	2.5	14.472	2.620
	40×40	−2.5	13.587	3.563	2.5	14.503	2.616
2:1	$60 \times 30^*$	−2.5	14.788	4.233	2.5	15.861	2.932
	80×40	−2.5	14.811	4.221	2.5	15.884	2.930
5:1	$100 \times 20^*$	−2.5	18.084	5.999	2.5	19.382	4.377
	150×30	−2.5	18.156	5.994	2.5	19.455	4.373
1:2	$30 \times 60^*$	−2.5	15.140	3.804	2.5	15.677	3.159
	40×80	−2.5	15.162	3.802	2.5	15.699	3.158
1:5	$20 \times 100^*$	−2.5	18.740	5.068	2.5	19.040	4.754
	30×150	−2.5	18.812	5.070	2.5	19.112	4.756

Table 3
Influence of grid size on *Nu* and *fRe* for a trapezoidal duct ($b/h = 1:1$) with base angle 60°

Grid	*fRe*	Nu_T	Nu_q	Nu_f
90×30	14.281	2.813	3.450	3.056
120×40	14.255	2.816	3.454	3.059
150×50	14.237	2.819	3.457	3.062
180×60	14.223	2.821	3.459	3.064
210×70	14.213	2.822	3.461	3.065

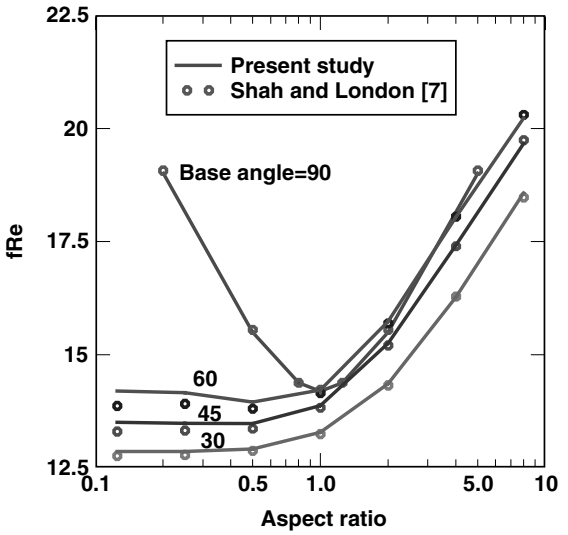

Fig. 2. Test results of the friction *fRe* as function of aspect ratio for rectangular (90°) and trapezoidal (30°, 45°, 60°) ducts.

boundary conditions. It is evident that the *Nu* for either constant heat flux, q_w, or constant temperature, T_w, on all the walls agree excellently with the analytical results from the literature [7]. The *Nu* for ducts with combined thermal boundary conditions are also shown in these figures.

If the aspect ratio of rectangular ducts goes to zero, the calculation results for the combined wall boundary conditions are similar to the results of constant wall temperature, which can be seen in Fig. 3(a). However, if the aspect ratio approaches infinity, the calculation results for the combined wall boundary conditions will be the average of the results for constant heat flux and constant temperature at all walls. These conclusions are true as Fig. 1(b) is considered.

As there are no available data so far in the literature for verification of the friction factor and *Nu* number when mass transfer is included, calculations have been carried out for square ducts ($b/h = 1:1$) with various injection rates under the boundary condition implemented by Hwang et al. [14]. The calculated results are shown in Fig. 4. The agreement between our calculations and the results obtained by Hwang et al. is satisfactory and the maximum deviation is about 5%.

The test calculations performed and discussed above show that the deviations of the calculated results from those presented in the literature are sufficiently small. Thus it is reasonable to believe that the numerical method and code can be used for the present study with satisfactory accuracy. The importance of the real thermal boundary conditions was also revealed.

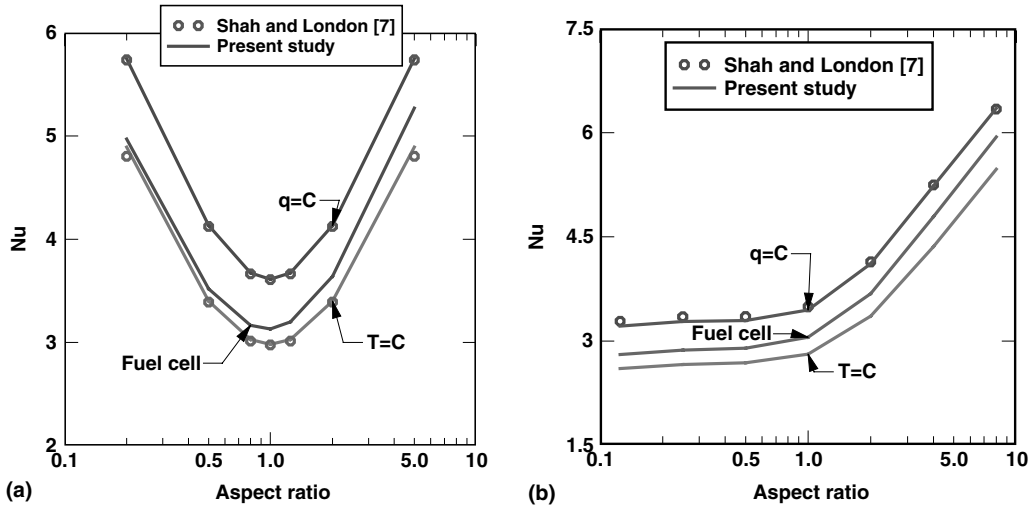

Fig. 3. Calculation results of *Nu* as function of aspect ratio in: (a) rectangular ducts, and (b) trapezoidal ducts with base angle 60°.

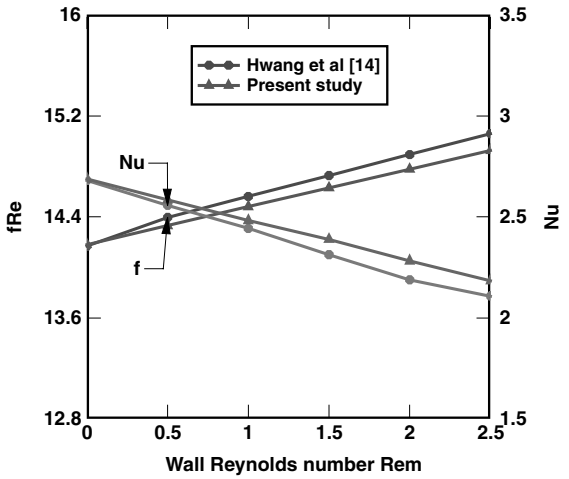

Fig. 4. Friction factor and *Nu* in square ducts including mass transfer. Boundary conditions according to Hwang et al. [14].

5. Results and discussion

To explore the flow and heat transfer characteristics, the effects of mass transfer on the fully developed laminar flow in rectangular and trapezoidal ducts are presented and discussed in this section. The flow friction factors and Nusselt numbers for various wall Reynolds numbers, aspect ratios and base angles are described and compared with existing data from the literature. The properties of H_2O and O_2 at a temperature of 1000°C (in SOFC) are chosen for the calculation of mass injection and suction, respectively, in this study.

5.1. Rectangular duct

5.1.1. The axial velocity and friction

For the injection, the mass transfer from the lower porous wall induces additional mass into the duct, and thus the axial velocity increases. For larger Re_m, more mass is injected and the increment at increase of the axial velocity is bigger. Because the lower porous wall is longer for the larger aspect ratio, more mass will be injected to the duct and a greater significant effect on the axial velocity gradient at a fixed Re_m will occur.

For the case of suction, the mass transfer induces mass flow reduction in the duct, and thus the axial velocity decreases. Higher suction rate at bigger Re_m and larger aspect ratio will have greater effect on the axial velocity decrease. Due to effects caused by a strong extraction flow, the rate of replenishment by the fluid in the cross-section may not be sufficient and flow reversal has in fact been found for a square duct flow at a critical wall Reynolds number ($Re_m = -11.5$) [14]. Thus fully developed flow cannot be reached at or beyond this critical suction rate. This means that the complete governing equations have to be solved instead.

In the case of mass transfer, the wall friction factor is related to the pressure gradient as well as changes in the momentum flux in the main flow direction [15]. The momentum flux changes with the mass transfer rate Re_m and the geometry of the duct. This can be understood from Eq. (13), and implemented by a modified pressure gradient dP/dz. The fully developed friction factor for both injection and suction flow with various aspect ratios are presented in Fig. 5.

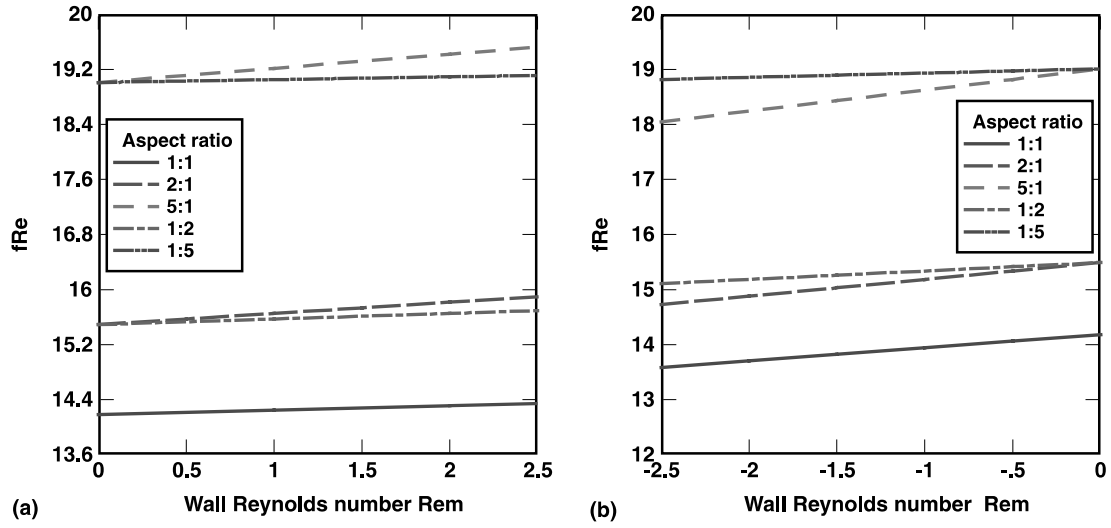

Fig. 5. Friction factor for a rectangular duct as function of mass transfer: (a) mass injection ($Re_m > 0$), and (b) mass suction ($Re_m < 0$).

For a fixed aspect ratio (see Fig. 5), the friction factor *fRe* always increases with mass injection and decreases with mass suction. A large aspect ratio can also contribute to a larger axial velocity gradient due to the fact that the mass transfer takes place at the lower wall. The friction factors of ducts with larger aspect ratios (2:1, 5:1) change more sharply with mass transfer rate, while for smaller aspect ratios (1:2, 1:5) the friction factor changes more smoothly with mass transfer rate.

5.1.2. Nusselt number

For the low injection and suction rate, the temperature profiles are not only similar to each other, but also invariant as the flow moves along the channel [14]. Attention is now focused on the so-called thermally fully developed regime within the fluid.

For injection flows, the temperature of the fluid will increase due to heat flux q_m, induced by mass injection into the fluid. For a constant aspect ratio, a larger amount of added heat is found at larger Re_m. The Nusselt number is thus reduced by mass injection which can be observed in Fig. 6(a). In the case of $Nu = 0$, all the heat transferred to the flowing fluid is from the mass transfer. As part of the thermal energy is carried away by the extracted mass, the temperature difference of the heated wall and bulk fluid is reduced by suction mass transfer. For a fixed aspect ratio, the stronger the suction is, the larger the Nusselt number is. This is shown in Fig. 6(b). A larger aspect ratio can also contribute to a higher heat flux q_m due to the fact that the mass transfer occurs on the lower wall, and a sharp change of the *Nu* for larger aspect ratios (2:1, 5:1) is found in Fig. 6.

Fully developed friction factors and Nusselt numbers as functions of various aspect ratios for both injection and suction flow are presented in Fig. 7. As can be seen, a larger aspect ratio has more significant effects on both *fRe* and *Nu*, while a smaller aspect ratio gives less effect. Both *fRe* and *Nu* approach the values for the case without mass transfer ($Re_m = 0$), if the aspect ratio becomes about 0.1. For a fixed aspect ratio, the Nusselt number is reduced by fluid injection and is increased by fluid suction. For the suction case with large aspect ratio, more thermal energy is supplied to the flow by the walls. Thus larger *Nu* have been observed as shown in Fig. 7(b). The figures also show that the friction factor and *Nu* have a minimum when the aspect ratio is unity, i.e., a square duct. Therefore it is desirable to find an optimal aspect ratio for which the heat transfer is large and the friction factor is small. Such a study is possible when additional information is available, e.g., maximum allowed friction factor, manufacturing aspects, etc.

5.2. Trapezoidal duct

Simulations with trapezoidal ducts have been carried out for different aspect ratios, base angles and wall Reynolds numbers. Figs. 8 and 9 show the results for *fRe* and *Nu* as function of different mass transfer rates for the aspect ratio 1:1. For a fixed base angle, the results follow those of rectangular ducts. With mass injection through the lower wall, the friction factor will increase while the *Nu* number is decreased, see Fig. 8. The highest friction factor occurs when the trapezoidal duct has a 60° base angle, while the highest *Nu* is for the square duct.

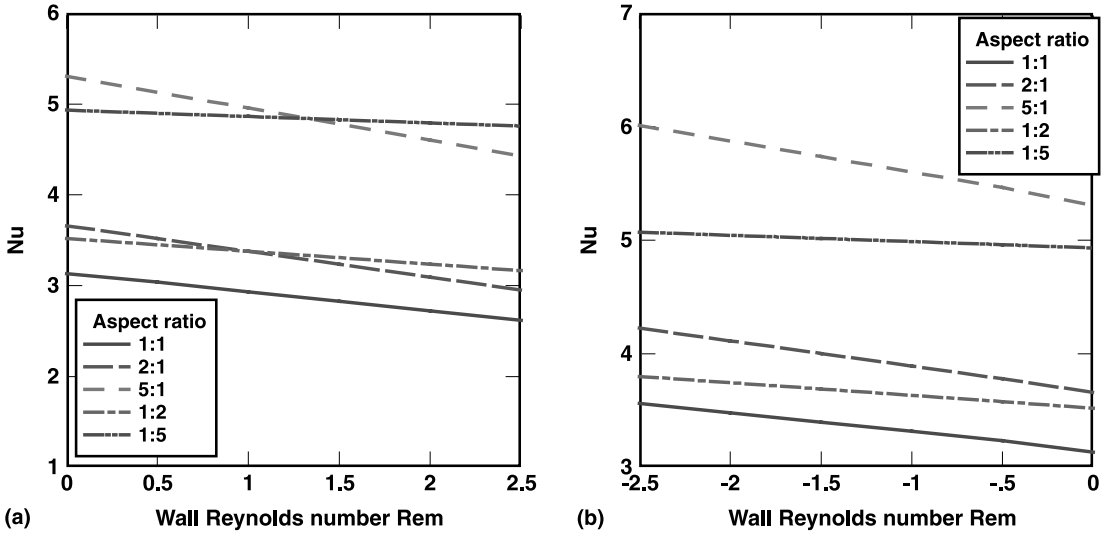

Fig. 6. Nusselt numbers of a rectangular duct as function of mass transfer: (a) mass injection ($Re_m > 0$), and (b) mass suction ($Re_m < 0$).

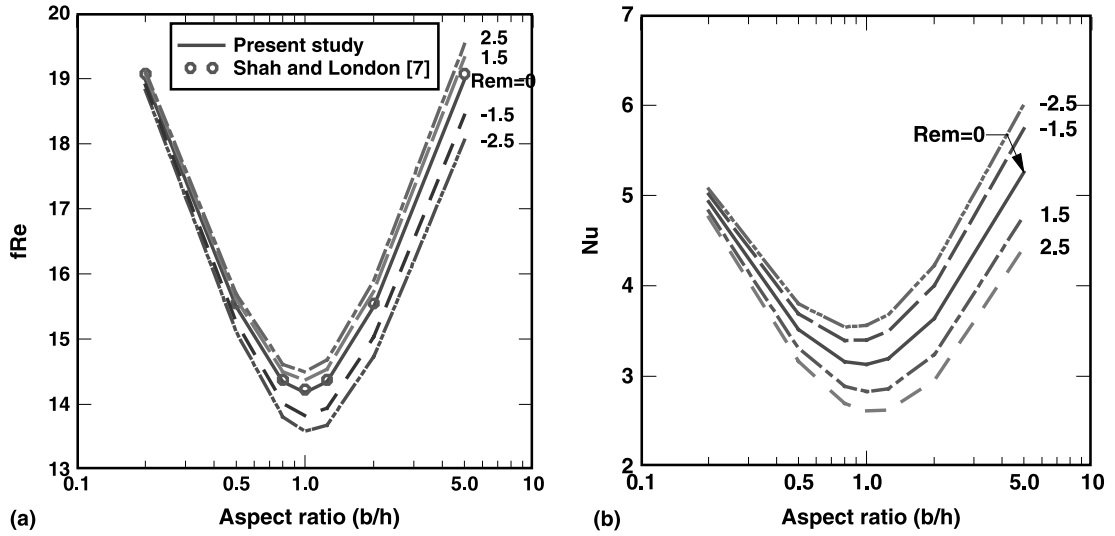

Fig. 7. Calculated friction factor *fRe* and Nusselt number in a rectangular duct as function of aspect ratio.

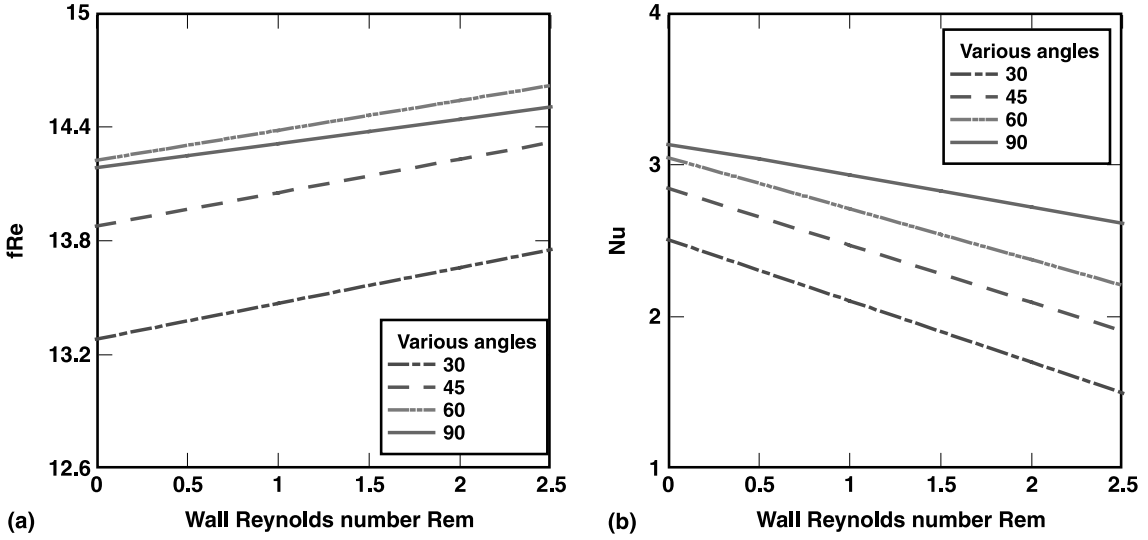

Fig. 8. Calculated friction factor and *Nu* in trapezoidal ducts with aspect ratio 1:1 as function of mass injection ($Re_m > 0$).

However, in the case of suction, the friction factor will be decreased while the *Nu* will be increased, see Fig. 9. The same conclusion (in terms of highest friction factor and *Nu*) as was drawn for the case of mass injection cannot be drawn here.

The figures also show that the friction factor and the *Nu* in trapezoidal ducts with different base angles change more sharply compared to rectangular ducts, when the wall Reynolds number Re_m changes.

To check the influence of the aspect ratio for a trapezoidal duct while keeping the base angle constant, Fig. 10 at an injection rate of $Re_m = 2.5$ is provided.

The results reveal that, with mass injection the friction factor and the *Nu* number are almost independent of the aspect ratio for small base angle less than 45°, and when the aspect ratio is less than unity. This was not the case for a rectangular duct, see base angle 90° in Fig. 10.

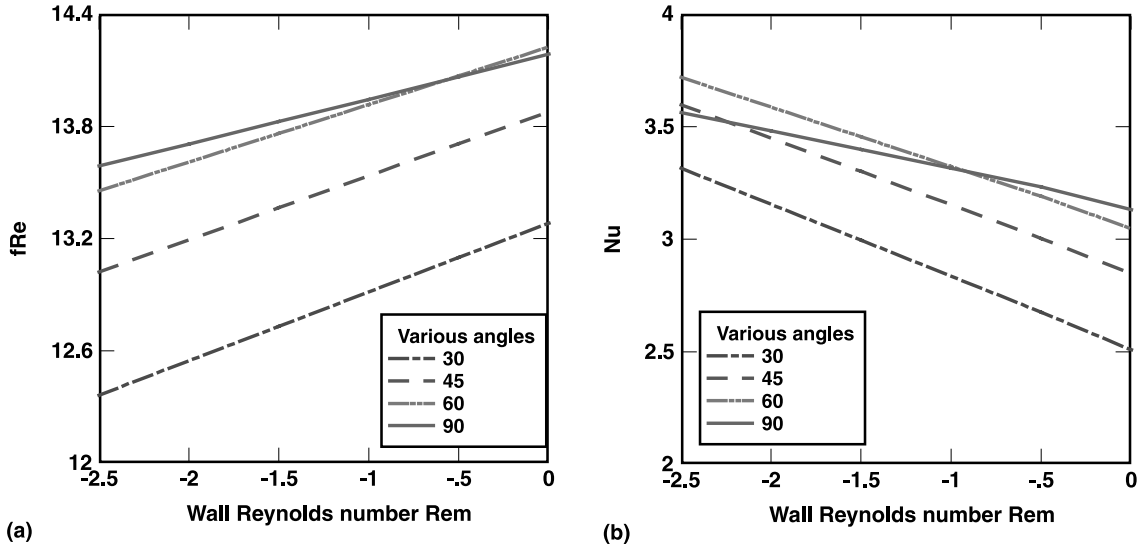

Fig. 9. Calculated friction factor and *Nu* in trapezoidal ducts with aspect ratio = 1:1, as function of mass suction ($Re_m < 0$).

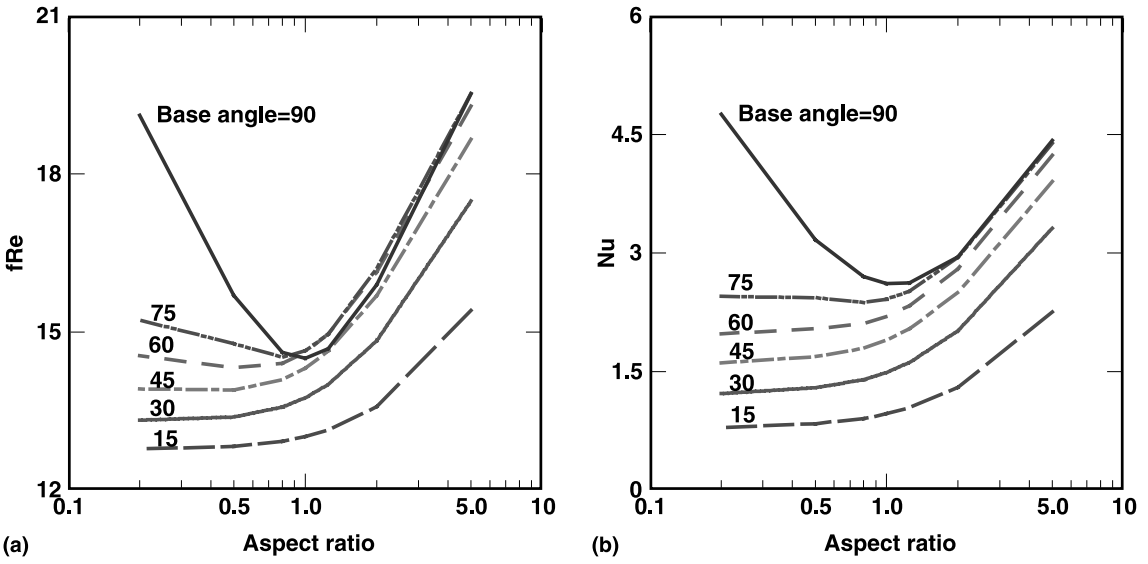

Fig. 10. Calculated friction factor and *Nu* in trapezoidal ducts as function of aspect ratio. The mass injection rate is $Re_m = 2.5$.

The base angle effect on the trapezoidal duct is shown in Fig. 11. It is evident that with mass injection both the friction factor and the *Nu* increase by increasing the base angle while keeping the aspect ratio constant. It is also found that a small base angle has greater effects for ducts with larger aspect ratios, while a large base angle has greater effects on ducts with small aspect ratios, as shown in Fig. 11. It should also be mentioned that these parameters approaches a certain value asymptotically as the base angle increases.

6. Conclusions

Numerical simulations of fully developed laminar flow and heat transfer for ducts with rectangular and

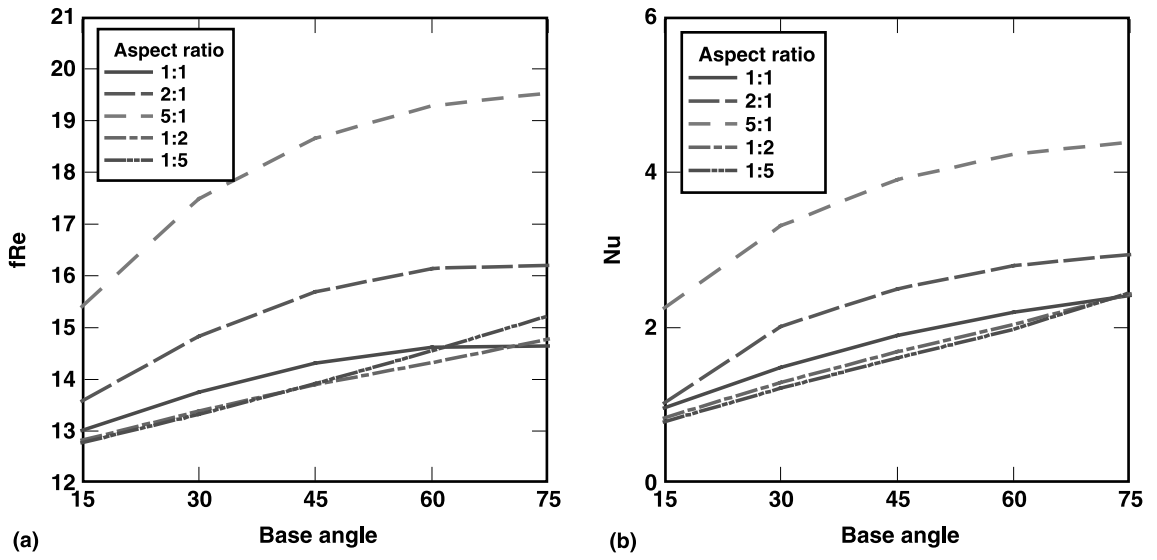

Fig. 11. Calculated friction factor and *Nu* in trapezoidal ducts as function of base angle. The mass injection rate is $Re_m = 2.5$.

trapezoidal cross-sections have been presented. One porous wall subject to a uniform mass flow and a new thermal boundary condition of combined constant heat flux at one wall and constant temperature at the other three walls were considered.

The presented numerical method was applied to ducts with constant wall temperature and constant wall heat fluxes (to verify its accuracy) and excellent results were obtained in terms of thermal–hydraulic parameters.

The model was also applied to the unique thermal boundary conditions of combined constant heat flux at one wall and constant temperature at the other three walls, which are thought to be close to the real situation in fuel cells. Also different ducts of rectangular and trapezoidal cross-sections were simulated.

It is found that the mass injection through one wall increases the friction factor and decreases the Nusselt number. The mass suction decreases the friction factor but the Nusselt number increases.

It has also been verified that mass transfer rate (Re_m), aspect ratio (b/h) and base angle have significant effects on the thermal–hydraulic parameters (friction factor and Nusselt number). However, the presented model is valid for small mass transfer Re_m less than about 2.5. This covers the mass transfer rates for SOFC ducts.

Acknowledgements

The present work is included in the national Swedish Programme for Stationary Fuel Cells. It is financially supported by the Swedish Energy Administration (STEM).

References

[1] A.V. Virkar, K. Fung, S.C. Singhal, The effect of pressure on solid oxide fuel cell performance, DOE Report, DOE/FETC/C-98/7303, December 1997.

[2] M. Bernier, J. Ferguson, R. Herbin, A 3-dimensional planar SOFC stack model, in: Proceedings of Third European Solid Oxide Fuel Cell Forum, Nantes, France, 1998, pp. 471–480.

[3] M. Rokni, B. Sundén, A numerical investigation of turbulent forced convection in ducts with rectangular and trapezoidal cross-section area by using different turbulence models, Numer. Heat Transfer 30 (1996) 321–346.

[4] M. Rokni, A new low-Reynolds version of an explicit algebraic stress model for turbulent convective heat transfer in ducts, Numer. Heat Transfer 37 (2000) 331–363.

[5] R.K. Shah, M.S. Bhatti, Laminar convective heat transfer in ducts, in: S. Kakac, R.K. Shah, W. Aung (Eds.), in: Handbook of Single-Phase Convective Heat Transfer, Wiley, New York, 1987.

[6] M.S. Bhatti, R.K. Shah, Turbulent and transition flow convective heat transfer in ducts, in: S. Kakac, R.K. Shah, W. Aung (Eds.), in: Handbook of Single-phase Convective Heat Transfer, Wiley, New York, 1987.

[7] R.K. Shah, A.L. London, Laminar flow forced convection in ducts, in: T.F. Irvine, J.P. Hartnett (Eds.), in: Advances in Heat Transfer, Academic Press, New York, 1978 (Chapters VII and X).

[8] C.G. Vayenas, P.G. Debenedettl, I. Yentekakls, L.L. Hegedus, Cross-flow, solid-state electrochemical reactors:

a steady-state analysis, Ind. Eng. Chem. Fundam. 24 (1985) 316–324.
[9] S. Ahmed, C. McPheeters, R. Kumar, Thermal–hydraulic model of a monolithic solid oxide fuel cell, J. Electrochem. Soc. 9 (138) (1991) 2712–2718.
[10] J.R. Ferguson, J.M. Fiard, R. Herbin, Three-dimensional numerical simulation for various geometries of solid oxide fuel cells, J. Power Sources 58 (1996) 109–122.
[11] O. Melhus, S.K. Ratkje, A simultaneous solution of all transport processes in a solid oxide fuel cell, Denki Kagaku 6 (64) (1996) 662–673.
[12] P. Costamagna, E. Arato, E. Achenbach, U. Reus, Fluid dynamic study of fuel cell devices: simulation and experimental validation, J. Power Sources 52 (1994) 243–249.
[13] R.J. Boersma, N.M. Sammes, Distribution of gas flow in internally manifolded solid oxide fuel-cell stacks, J. Power Sources 66 (1997) 41–45.
[14] G.J. Hwang, Y.C. Cheng, M.L. Ng, Developing laminar flow and heat transfer in a square duct with one-walled injection and suction, Int. J. Heat Mass Transfer 9 (36) (1993) 2429–2440.
[15] R.B. Kinney, Fully developed frictional and heat-transfer characteristics of laminar flow in porous tubes, Int. J. Heat Mass Transfer 11 (1968) 1393–1401.
[16] J.P. Quaile, E.K. Levy, Laminar flow in a porous tube with suction, Trans. ASME J. Heat Transfer 97 (1975) 66–71.
[17] J. Yuan, M. Rokni, B. Sundén, The development of heat transfer and gas flow modeling in the solid oxide fuel cells, in: S.C Singhal, M. Dokiya (Eds.), in: Solid Oxide Fuel Cells (SOFC VI), The Electrochemical Society, Pennington, 1999, pp. 1099–1108.
[18] H.K. Versteeg, W. Malalasekera, An Introduction to Computational Fluid Dynamics, The Finite Volume Method, Longman Scientific & Technical, England, 1995.
[19] B. Sundén, M. Rokni, M. Faghri, D. Eriksson, The Computer Code SIMPLE_HT, No 98/2, Lund Institute of Technology, Lund, 1998.
[20] G.D. Raithby, G.E. Schneider, Elliptic systems: finite difference method II, in: W.J. Minkowycz, E.M. Sparrow, G.E. Schneider, R.H. Pletcher (Eds.), in: Handbook of Numerical Heat Transfer, Wiley, New York, 1988 Chapter 7.
[21] S.V. Patankar, Numerical Heat Transfer and Fluid Flow, McGraw-Hill, New York, 1980.